THE JOURNAL OF PHYSICAL CHEMISTRY A

Article

pubs.acs.org/JPCA

Substitutional Photoluminescence Modulation in Adducts of a Europium Chelate with a Range of Alkali Metal Cations: A Gas-Phase Study

Jean-Francois Greisch,*[,†] Michael E. Harding,[†] Bernhard Schäfer,[†] Martin Rotter,[‡] Mario Ruben,[†,§] Wim Klopper,[†,∥] Manfred M. Kappes,[†,∥] and Detlef Schooss*[,†,∥]

[†]Institute of Nanotechnology, Karlsruhe Institute of Technology (KIT), Hermann-von-Helmholtz-Platz 1, 76344 Eggenstein-Leopoldshafen, Germany

[‡]Max Planck Institute for Chemical Physics of Solids, Nöthnitzer Strasse 40, 01187 Dresden, Germany

[§]Institut de Physique et Chimie des Matériaux de Strasbourg (IPCMS), CNRS-Université de Strasbourg, 23, rue du Loess, BP 43, 67034 Strasbourg cedex 2, France

[∥]Institute of Physical Chemistry, Karlsruhe Institute of Technology (KIT), Fritz-Haber-Weg 2, 76131 Karlsruhe, Germany

Supporting Information

ABSTRACT: We present gas-phase dispersed photoluminescence spectra of europium-(III) 9-hydroxyphenalen-1-one (HPLN) complexes forming adducts with alkali metal ions ($[Eu(PLN)_3M]^+$ with M = Li, Na, K, Rb, and Cs) confined in a quadrupole ion trap for study. The mass selected alkali metal cation adducts display a split hypersensitive $^5D_0 \rightarrow {}^7F_2$ Eu^{3+} emission band. One of the two emission components shows a linear dependence on the radius of the alkali metal cation whereas the other component displays a quadratic dependence thereon. In addition, the relative intensities of both components invert in the same order. The experimental results are interpreted with the support of density functional calculations and Judd−Ofelt theory, yielding also structural information on the isolated $[Eu(PLN)_3M]^+$ chromophores.

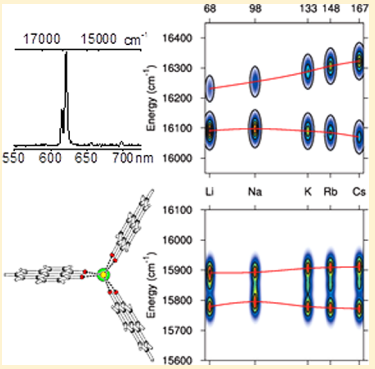

INTRODUCTION

Lanthanoid containing molecular complexes have found a wide range of applications including organic electroluminescence,[1,2] photovoltaic cell enhancement,[3,4] and fluoroimmunoassays.[5] Compared to standard chromophores, their emission is relatively insensitive to the environment because it arises from 4f−4f transitions. The effective shielding of the 4f electrons by the filled $5s^25p^6$ subshells as well as the parity forbidden character of the electric dipole 4f → 4f transitions govern the photophysical properties of lanthanoid emitters.[6,7] This results in characteristic narrow-line emission bands, relatively long luminescence lifetimes ranging from microseconds to milliseconds,[8] and extinction coefficients on the order of 1 M^{-1} cm^{-1} for bare ions, 3−5 orders of magnitude smaller than those of conventional organic chromophores.[7] To circumvent the ineffective direct excitation, organic or metal−organic coordinative ligands characterized by a high molar absorptivity are often used as light absorbing species with the energy subsequently intramolecularly transferred to the lanthanoid. This process is known as sensitization or the antenna effect.[7,9] The mechanisms proposed to account for the sensitization of homonuclear lanthanoid complexes are typically discussed in terms of localized ligand/lanthanoid based states. For organic ligands, the most commonly accepted mechanisms are electronic energy transfer from the triplet excited state of a conjugated ligand via a Dexter-like[10−16] or superexchange mechanism;[17,18] energy transfer involving intraligand charge transfer (ILCT) states, either associated with a singlet excited state pathway or collapsing to a triplet state acting as the ultimate sensitizer state;[19−25] and a stepwise double-electron-transfer pathway between the ligand and the lanthanoid (LMLCT), for the most readily reduced lanthanoids, e.g., Eu^{3+}, Yb^{3+}, Sm^{3+}, and Tm^{3+}.[26−28] For transition metal containing ligands there are additional possible mechanisms including an energy transfer process involving triplet metal-to-ligand charge transfer (^{3}MLCT) states with the metal ions sometimes additionally contributing to the efficient intersystem crossing to the triplet state of the energy-donor via the so-called "heavy atom effect".[1,29−34] In some cases relaxation to a metal centered excited state also takes place and is followed by a Förster like energy transfer to the lanthanoid ion.[35−37]

Sensitized Eu(III) typically emits from one of its two well established emitting states, the $^5D_0$ and $^5D_1$ levels, respectively, at 17 250 and 19 000 cm^{-1} compared to the $^7F_0$ ground state.[38]

Received: August 29, 2013
Revised: December 14, 2013
Published: December 16, 2013

Although some of the 4f → 4f transitions are electric quadrupole or magnetic dipole parity allowed, the observed intensities can only be accounted for by electric dipole contributions.[39−41] The relaxation of Laporte's rule involves noncentrosymmetric electric fields generated by the coordinating ligands, geometry fluctuations of the ligand shell/field caused by vibrations, J-mixing or the mixing of states with opposite parity involving, e.g., 5d orbitals or ligand orbitals.[42−49] The 9-hydroxy-phenalen-1-one (HPLN) ligand was selected for its high absorption cross section ranging from the near-UV to 475 nm in the condensed phase,[50] its long-lived ($\tau \sim 25$ ms) phosphorescence with origin near 17 350 cm^{-1},[51] and its ability to coordinate lanthanoids and transfer energy to coordinated europium atoms.[52]

This work is part of a systematic study of the intrinsic properties of photoluminescent ionic chromophores in the gas phase using mass spectrometric techniques.[53] It aims at a better understanding of the interactions between these chromophores and their environment via direct comparison between measurements and model computations, focusing in particular on effects that allow the emission properties to be modified by design. Inherent to this approach is the knowledge of the exact stoichiometry of the noncovalent or coordinative complexes studied. This is a significant advantage compared to solution measurements for which the exact stoichiometry of the species present is often not known and regulated by equilibria. The present study is the first to make use of such mass spectrometric capabilities to select and study the luminescence properties of isolated europium complexes.

Different experimental setups have been developed for gas-phase laser induced fluorescence measurements on trapped molecular ions. They include ion cyclotron resonance cells,[54,55] linear quadrupole traps,[56] and quadrupole ion traps.[57−60] Up to now the focus has been almost exclusively on rhodamine and similar organic fluorophore cations because of their high fluorescence quantum yields, high absorption cross sections and high photostabilities at commonly available laser wavelengths. The present paper focuses on a range of photoluminescent Eu(III) complexes cationized for mass spectrometric study by adduct formation with alkali metal ions. Specifically, we have studied how different alkali-metal ions influence the emission properties of the respective adduct species. Systematic, alkali-cation-dependent trends in the splitting of Eu(III) emission are uncovered and related to ligand field effects with the help of quantum chemical calculations.

EXPERIMENTAL AND THEORETICAL METHODS

Sample Preparation. All reagents and solvents used in this study are commercially available and were used without any further purification. Infrared spectra were recorded using KBr-pressed pellets with a Perkin-Elmer Spectrum GX FT-IR spectrometer. Elemental analyses were carried out on a Vario Micro Cube.

$Eu(PLN)_3$ was prepared as described before.[52] Yield: 0.139 g (51%). Elemental analysis (%) calculated for ($C_{39}H_{21}EuO_6 \cdot 3H_2O$): C, 59.09; H, 2.89. Found: C, 59.17; H, 3.44. FT IR (KBr): 3432, 1631, 1588, 1561, 1521, 1428, 1425, 1402, 1385, 1347, 1257, 1242, 1181, 1139, 986, 852, 745, 484, 452 cm^{-1}.

$Na[Eu(PLN)_4]$ and $K[Eu(PLN)_4]$ have not been previously reported. They were prepared following a modified literature procedure using $Eu(H_2O)_6Cl_3$ instead of $YbCl_3$ as used by Van Deun et al. to prepare $M[Yb(PLN)_4]$.[61]

$K[Eu(PLN)_4]$: HPLN (0.2 g, 1 mmol, 4 equiv) was suspended in EtOH (50 mL), and a solution of KOH (0.152 g, 2.7 mmol, 2.7 equiv) in 2 mL water was added. The suspension was stirred and heated with an oil bath (T = 328K). After 1 h, a solution of $Eu(H_2O)_6Cl_3$ (93.3 mg, 0.254 mmol, 1 equiv) in EtOH was added. The reaction was allowed to proceed overnight (17 h). The heater was then switched off and the product was collected by filtration (after 5 h standing at room temperature). The precipitate was washed three times with 1 mL of water and dried at a membrane pump yielding 0.22 g of product (86%). Elemental analysis (%) calculated for $M \cdot 2H_2O$ ($C_{52}H_{32}EuKO_{10}$): C, 61.97; H, 3.20. Found: C, 62.12; H, 3.26. FT IR (KBr): 3437, 1630, 1587, 1559, 1523, 1429, 1414, 1385, 1349, 1253, 1242, 1179, 1148, 985, 852, 844, 745, 481, 447 cm^{-1}.

$Na[Eu(PLN)_4]$: The reaction was carried out as described for $K[Eu(HPLN)_4]$ but NaOH was used instead of KOH. Yield: 0.2 g (81%). Elemental analysis (%) calculated for $M \cdot H_2O$ ($C_{52}H_{30}EuNaO_9$): C, 64.14; H, 3.11. Found: C, 63.80; H, 3.20. FT IR (KBr): 3434, 1629, 1586, 1559, 1527, 1431, 1413, 1349, 1253, 1242, 1179, 1150, 986, 851, 745, 482, 450 cm-1.

The ^1H NMR spectrum of a $Eu(PLN)_3$ sample was measured in DMSO-d_6 (Figure SI-2, Supporting Information). In comparison to the free HPLN ligand the proton signals of the $Eu(PLN)_3$ complex are shifted to higher fields. The four resonances expected for PLN are observed, indicating that the three PLN ligands in the complex are chemically equivalent. As reported in the literature for Y-complexes of PLN, an additional signal set is also observed with an intensity of one-ninth compared to the $Eu(PLN)_3$ signals.[61] This could be evidence of the complex involvement in a dynamical equilibrium, these signals being similar to those of the $Na[Eu(PLN)_4]$ complex. A dynamical equilibrium involving DMSO and water adducts of the $Eu(PLN)_3$ complex, e.g., $[Eu(PLN)_3(DMSO)_2]$ and $[Eu(PLN)_3(H_2O)_2]$, is also possible.

Structure and Energy Level Modeling Using Density Functional Computations and Judd−Ofelt Theory. The structures of the complexes were initially explored at the PM6-SPARKLE level.[62] Following this first step, the structures and the electron densities used for population analysis were computed using density functional theory (DFT) employing the B-P functional[63] in combination with the def2-TZVPP basis set[64−66] as implemented in the TURBOMOLE program package.[67] The resolution-of-identity (RI) approximation was applied in all calculations.[64,68] A self-consistent-field convergence threshold of 10^{-8} hartree and geometry convergence thresholds of 10^{-8} hartree and 10^{-5} hartree/bohr for the total energy and the Cartesian gradient, respectively, were used. The numerical quadrature was performed on TURBOMOLE's grid 5. These computations do not include spin−orbit coupling effects nor do they allow for a direct assessment of the Stark splitting of the europium energy levels by the ligand field. Geometry optimizations have been carried out for both the ^7F and the ^5D states and the structures are found to be in reasonable agreement (about ±5 pm difference in Eu−alkali and Eu−O distances). The *xyz*-coordinate files of all structures presented in this work are provided as Supporting Information. Due to the facts that the ^5D state cannot be represented properly by a single reference determinant and that the ^7F state appears to be qualitatively accessible via an unrestricted single determinant Ansatz, the latter seems to be the preferred choice. Therefore, in the following only results for the ^7F ground state

dx.doi.org/10.1021/jp4086624 | J. Phys. Chem. A 2014, 118, 94−102

geometry of the molecules will be presented although the emission originates from the ^5D state.

A Eu^{3+} ion in free space has spherical symmetry, and each energy level is characterized by its total angular momentum J, which is $(2J + 1)$-fold degenerated. When Eu^{3+} is placed in a ligand field, the degeneracy is at least partly lifted depending on the point-group symmetry of the ion surroundings.[69] To simplify the resulting Hamiltonian, the ligands can be replaced by point charges generating a ligand electrostatic field that upon interaction with the 4f electrons induces a Stark splitting of the corresponding spectroscopic levels. The ligand-field perturbation that accounts for the experimentally observed splitting of the 4f–4f hypersensitive band $^5D_0 \rightarrow {}^7F_2$ can be expressed, following Wybourne's formalism, as $H_{LF} = \sum_{k,q,i} B_q^k C_q^{(k)}(i)$ where the B_q^k are ligand-field parameters, the $C_q^{(k)}$ are components of a tensor operator $C^{(k)}$ that transforms like the spherical harmonics used for the analytical form of the 4f orbitals and the summation involves all the 4f electrons of the ion of interest. If one neglects the coupling to states of opposite parity in higher lying configurations such as $4f^{(n-1)}5d$, the connected angular momenta, l and l', are equal to 3, and k is therefore limited to the even values 0, 2, 4, and 6. As part of the total Hamiltonian, H_{LF} exhibits the same symmetry as coordinated Eu^{3+} and q values are restricted to $|q| \leq k$, with the cases $|q| = 1$ and $|q| = 5$ occurring only when there is no symmetry, as for C_1. Finally, the term with $k = q = 0$ can be neglected because it only uniformly shifts all the levels in the configuration.[69,70] The McPHASE[71] *pointc* module was used to calculate the relevant real valued Wybourne normalized ligand-field parameters (L_{kq}, appendix D.4 in ref 71) from the natural population analysis (NPA)[72] point charges computed using B-P/def2-TZVPP. Point charge population analysis typically retains some arbitrary character,[73] and europium point charges were found to differ from the expected charge (+3) independent of the point charge model used. Therefore, the europium(III) point charge was increased to +3 (the alkali charge was set to +1 although the difference from the computed NPA charge is negligible) and the compensating oxygen point charges were scaled correspondingly so as to retain a total charge of +1 for the whole complex. The Stark splitting of the $^7F_2$ level resulting from this ligand field as well as the related energy gaps were then evaluated using the *ic1ion* module of McPHASE.[71] Relative transition probabilities are currently not accessible computationally. Finally, to assess the limitations of the point charge analysis used, the NPA charges were also compared to Mulliken charges.

Experimental Characterization. The experimental setup is described in ref 60. In brief, gas-phase ions produced using a nanoelectrospray source are stored in a temperature regulated quadrupole ion trap held at 85 K throughout the experiment. Ions mass selected using the stored waveform inverse Fourier transform (SWIFT) method[74] are thermalized by collisions with a helium buffer gas at an approximate pressure of 0.2 mbar held constant during the accumulation of luminescence spectra. Under the experimental conditions (T = 85 K) a collision probability of ~10 MHz was estimated using the Langevin expression. For dispersed luminescence measurements, trapped ions (~10^4) are excited by the 458 nm line of a continuous wave (cw) Ar^+ laser (Spectra Physics 2080-15S) orthogonal to the ion trap axis. The laser beam is attenuated in discrete steps by means of neutral density filters, spectrally cleaned by a narrow band-pass filter (Semrock) and synchronized with the experiment using an electromechanical beam shutter. The laser beam is focused to the center of the ion trap by a f = 500 mm lens, passed through 1.2 mm holes in the ring electrode and finally dumped onto a photodiode for power measurement. At the trap center, the laser beam was measured to be 0.2 mm in diameter ($1/e^2$). Typical irradiances are ~1910 W/cm^2 for Li and Na adducts and ~480 W/cm^2 for K, Rb, and Cs. Ion luminescence is collected perpendicularly to the excitation beam by a microscope objective (Zeiss EC PlanNeofluor5x/0.15) through a 3 mm diameter aperture in one of the end caps. A long pass edge filter (Semrock) removes scattered excitation light before being focused into a fiber and sent to a spectrograph (Triax 190, 300 grooves/mm, Jobin-Yvon, Horiba or 300i, 150 grooves/mm, Acton Research, Roper Scientific) coupled to a CCD camera for detection (Newton DU970N-BV EMCCD, Andor, or Idus DV401-A-BV, Andor).

In preparation for electrospray, the Eu(III) complexes were dissolved in dimethyl sulfoxide (DMSO) to an approximate concentration of 10^{-4} M. As can be directly assessed from the positive ion mass spectrum of Figure 1, cationization typically involves adduct formation with either sodium or potassium ions depending on the inorganic base (NaOH or KOH) used during the synthesis. To generate other alkali metal adducts, sodium or potassium was displaced by adding 0.1% v:v of a saturated DMSO solution of the corresponding alkali metal iodide (LiI, RbI, CsI) to the stock solutions before electrospraying.

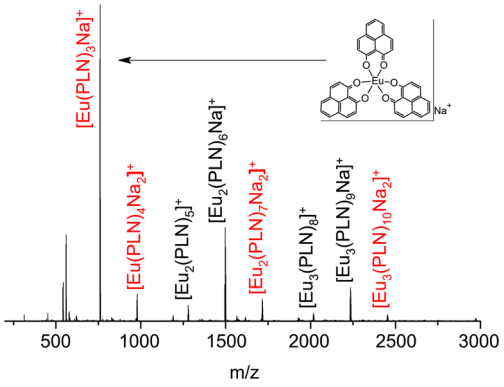

Figure 1. Positive ion mode mass spectrum of europium 9-hydroxyphenalen-1-one complexes electrosprayed from a DMSO solution (NaOH synthesis). The species highlighted in red luminesce strongly under 458 nm excitation.

RESULTS

Composition and Coordination. Europium(III) coordination by 9-hydroxyphenalen-1-one can lead to the formation of mononuclear $[Eu(PLN)_3]$ and $[Eu(PLN)_4]^-$ complexes. As seen upon electrospraying from solution, both of these can be easily cationized by one and two alkali metals, respectively. Figure 1 displays a typical positive ion mass spectrum also showing the corresponding alkali metal cation adducts (a negative ion mass spectrum can be found in Supporting Information). We mass selected the species of interest by removing all other ions from the trap to study their intrinsic photoluminescence properties separately. In this publication we will be concerned with those $[Eu(PLN)_3]$-derived species having highest relative abundance and strongest photoluminescence, i.e., $[Eu(PLN)_3M]^+$ (M = Li, Na, K, Rb, and Cs).

Essentially four families of $[Eu(PLN)_3M]^+$ structures have been identified by density functional calculations corresponding

dx.doi.org/10.1021/jp4086624 | J. Phys. Chem. A 2014, 118, 94–102

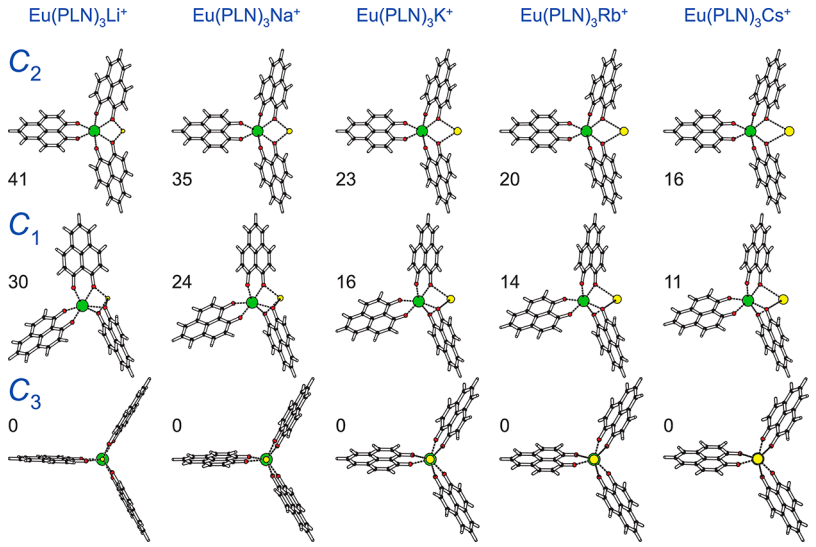

Figure 2. C_2, C_1, and C_3 symmetric structures optimized at the B-P/def2-TZVPP level together with their relative energies in kJ/mol (europium in green, alkali metal in yellow, oxygen atoms in red). In the C_3 case, the structures are propeller-like with the alkali metal sitting on the C_3 axis.

to C_1, C_2, C_3, and C_s symmetries. The C_s family was found to be either significantly higher in energy (~40−150 kJ/mol) or, for some of the alkali metal cations, to collapse to the C_3 family upon optimization. Therefore, only the first three types of isomers will be explicitly considered in the following (Figure 2). These families differ by their coordination shells and consequently by their ligand fields. The NPA charges were calculated for each structure and used to model the splitting of the hypersensitive band $^5D_0 \rightarrow {}^7F_2$.

The ion geometries can be described as follows: all of the complexes under study have a 6-fold oxygen-coordinated europium atom. The alkali metal is coordinated to three oxygen atoms in the C_3 and C_1 structures and to two oxygen atoms in the C_2 structures. The alkali metal−europium distances increase with both the ionic radius of the alkali metal and the coordination symmetry of the europium atom from (287−391 pm) for C_3 to (285−400 pm) for C_1 to (310−417 pm) for C_2. For a given symmetry, the B-P/def2-TZVPP alkali metal binding energies decrease from 349 to 139 kJ/mol for C_3, from 308 to 123 kJ/mol for C_2, and from 320 to 128 kJ/mol for C_1 in going from Li to Cs, respectively. The C_3 structures evolve from a slightly distorted triangular prism with one of the triangular bases smaller and slightly rotated (6°) compared to the other one for Li, to a distorted triangular antiprism (triangular bases rotated by −32°) for Cs. Equivalently, the ligands of the C_3 symmetric species show an increasing axial tilt with respect to the C_3 axis when going from Li (3°) to Cs (28°). For the species featuring a C_2 axis a nearly constant ligand opening angle of about 140° is found, whereas the almost planar ring systems of the ligands on the side of the alkali metal show a decreasing dihedral angle (81° (Li) to 52° (Cs)). The C_2 structures are best described as distorted octahedra. The angle subtended by the europium at the apex and the oxygen atoms approximately orthogonal to the plane defined by the alkali metal and its coordinating oxygen atoms, decreases monotonically from 168° for Li to 161° for Cs. The C_1 structures are strongly distorted intermediates between a triangular antiprism and an octahedron.

Dispersed Luminescence. Figure 3 shows typical dispersed luminescence measurements recorded in the 550−725 nm emission wavelength range upon 458 nm excitation.

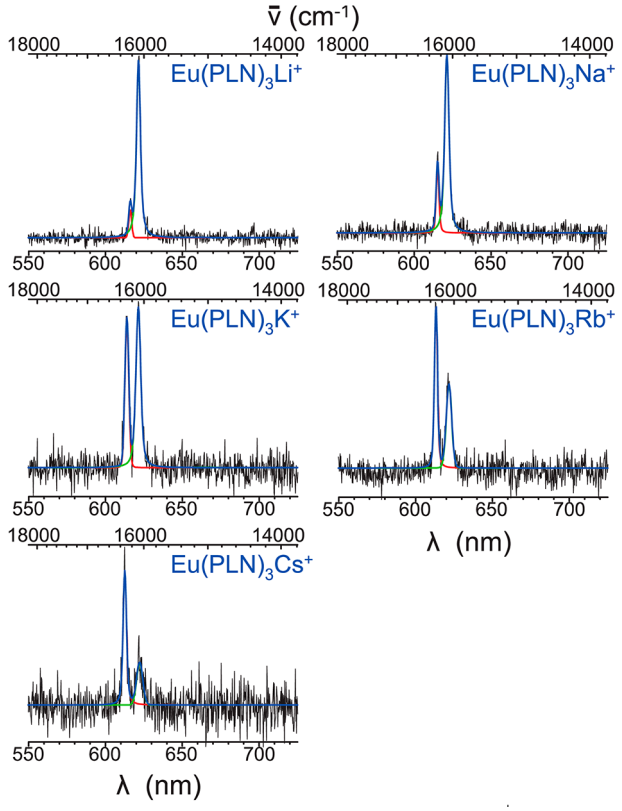

Figure 3. Dispersed luminescence spectra of the $[Eu(PLN)_3M]^+$ complexes with M = Li, Na, K, Rb, and Cs. Excitation 458 nm, temperature 85 K, He pressure ~0.2 mbar, typical combined acquisition durations ranged from 800 s for the particularly brightly emitting Li to 4800 s for Cs, laser irradiance ~1910 W/cm^2 for Li and Na; ~480 W/cm^2 for K, Rb, and Cs.

The spectra show a clear $^5D_0 \rightarrow {}^7F_2$ luminescence band split into a lower and a higher energy component. The extent of this $^5D_0 \rightarrow {}^7F_2$ hypersensitive band splitting changes systematically upon variation of the cation adduct from Li to Cs. Both components can be well fitted using Voigt functions. The line width (full width at half-maximum) range is typically [55; 80]

dx.doi.org/10.1021/jp4086624 | J. Phys. Chem. A 2014, 118, 94−102

cm^{-1} for the low energy component (E_1) and [80; 105] cm^{-1} for the high energy component (E_2). Resolution of finer spectral structures could not be achieved using our present experimental setup. A spectrum acquired with a coarser grating (see the Experimental Characterization section for more details) is displayed in Figure 4 for the $[Eu(PLN)_3Na]^+$

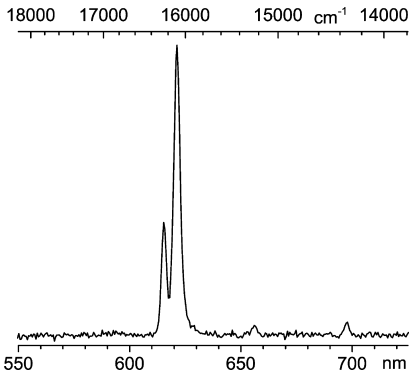

Figure 4. Dispersed luminescence spectrum of the $[Eu(PLN)_3Na]^+$ complex with improved signal-to-noise ratio. Excitation 458 nm, temperature 83 K, He pressure ~0.2 mbar, acquisition time 8000 s, laser irradiance ~1910 W/cm^2.

complex. Although the $^5D_0 \rightarrow {}^7F_3$ and $^5D_0 \rightarrow {}^7F_4$ transitions are now evident, no traces of the $^5D_0 \rightarrow {}^7F_0$ and $^5D_0 \rightarrow {}^7F_1$ transitions are detectable. This is not unexpected because the $^5D_0 \rightarrow {}^7F_1$ transition is typically weak in complexes of C_3 symmetry with polarizable ligands.[75,76]

Figure 5 illustrates how the energies of the two $[Eu(PLN)_3M]^+$ emission components depend on the ionic radius of the alkali metal involved. Of the four principal scales of ionic radii available in the literature, we chose to compare to Pauling crystal ionic radii because they are usually preferred for electrochemical and solvation problems.[77] The smaller the alkali-metal cation, the larger is the expected inductive effect on the ligated molecule. Note also that the first ionization energies of the alkali metal atoms (IE(M)) are linearly dependent on their ionic radius and therefore that a plot of transition energies versus IE(M) would look quite similar to Figure 5.

We observe a linearly increasing dependence of the transition energy of the higher energy emission component, E_1, on the ionic radius. In contrast, the lower energy component, E_2, displays a seemingly quadratic dependence of its transition energy on ionic radius (Figure 5a,b). Additionally, Figure 5c shows that the ratio of E_1 intensity ($I(E_1)$) to the total intensity of the $^5D_0 \rightarrow {}^7F_2$ hypersensitive band ($I(E_1) + I(E_2)$) also depends linearly on the ionic radii of the complexed alkali metal cations.

To facilitate comparison of model and experiment, we also summarize the experimental data in terms of a contour map showing transition energies and relative intensities together (Figure 6a). The corresponding theoretical energy splittings of the $^7F_2$ level calculated using McPHASE[78] for the geometries and NPA charges obtained at the B-P/def2-TZVPP level are displayed in Figure 6b–d. As already stated above, intensities cannot be obtained from these calculations. We therefore assume identical amplitudes and mimic the experimental broadening with appropriately scaled Gaussian functions. Their superposition yields the maxima displayed.

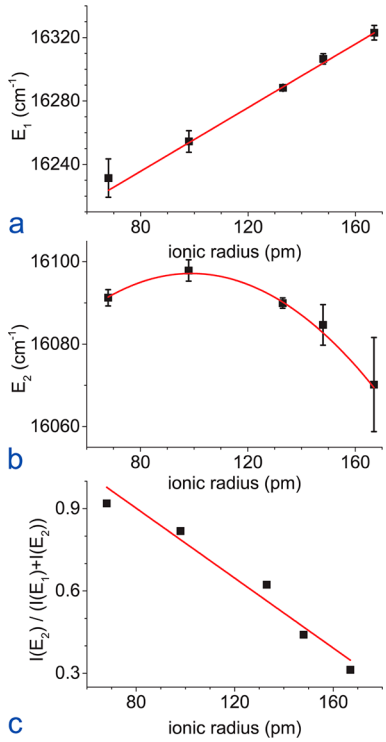

Figure 5. Energies of the emission band components for $[Eu(PLN)_3M]^+$ complexes, E_1 (a) and E_2 (b), as a function of the ionic radius of the alkali metal involved (M = Li, Na, K, Rb, and Cs); (c) ratio of the intensity of E_1 to the total intensity of the $^5D_0 \rightarrow {}^7F_2$ hypersensitive band. The error bars correspond to the standard error of the parameters extracted from the fit of the averaged data.

DISCUSSION

We have carried out measurements of the dispersed photoluminescence of mass-selected $[Eu(PLN)_3M]^+$ cations stored in a quadrupole ion trap (QIT) mass spectrometer to explore the effect of varying the alkali metal adduct (M = Li, Na, K, Rb, and Cs) on the emission spectra of the europium(III) coordination complex. We find the luminescence properties to be significantly dependent on the nature of the cations.

The spectra recorded in the emission wavelength range 550–725 nm show a dominant hypersensitive band ($^5D_0 \rightarrow {}^7F_2$ at about 612 nm), indicative of an asymmetric environment for the europium ion. Furthermore, the hypersensitive band is split into two components which are observed at about 16 090 and 16 300 cm^{-1} for all the alkali metal cation adducts studied (Figure 3). Both the intensity ratio of the two components and their respective spectral shifts show a systematic dependence on the size of the alkali metal cation involved (Figure 5).

Two different plausible scenarios are able to qualitatively explain the systematic variations induced by the alkali metal cations: (i) for each complex, two populations of isomers coexist with their proportion systematically shifting with the ionic radii of the cations or (ii) a single isomer population is always present and the observed splittings of the energy levels are instead the result of two groups of optical transitions with different probabilities of occurrence, one of which progressively takes over when the cations change from lithium to cesium. To further explore these scenarios, we have modeled the emission performing calculations on various structural candidates as described in detail above (Figure 6). We predict splittings and alkali metal dependent trends consistent with the single isomer

dx.doi.org/10.1021/jp4086624 | J. Phys. Chem. A 2014, 118, 94–102

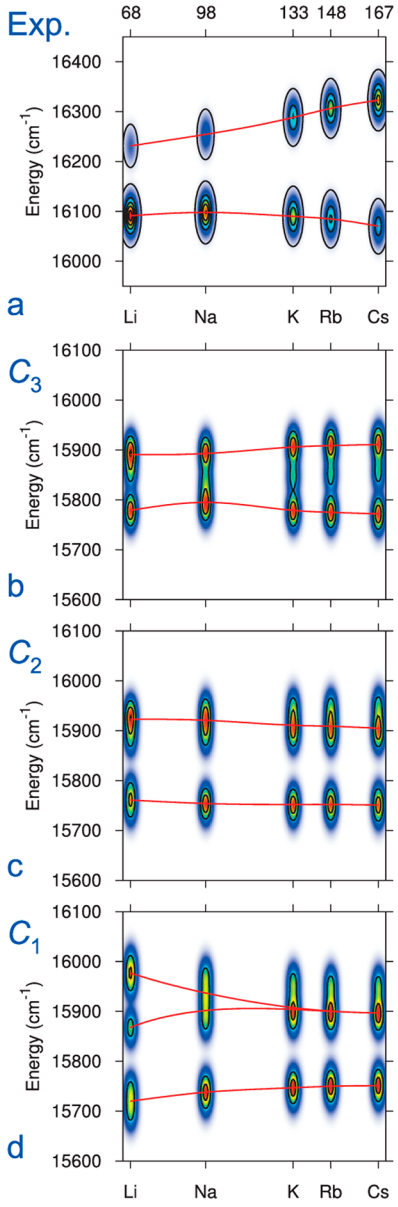

Figure 6. (a) Experimental band positions and relative intensities for the $^5D_0 \rightarrow {}^7F_2$ transitions of $[Eu(PLN)_3M]^+$ with M = Li, Na, K, Rb, and Cs. Splitting of the $^7F_2$ level calculated using McPHASE for the C_3 (b), C_2 (c), and C_1 (d) geometries and associated scaled NPA charges obtained at the B-P/def2-TZVPP level (see text). The red lines are splines used to highlight the trends.

hypothesis and therefore tend to rule out significant contributions from other spectrally distinct isomers simultaneously present. Note that an alternative explanation of the emission band splitting in terms of vibronic satellites is hard to reconcile with the systematic shifts in intensity from one emission component to the other observed upon changing M^+.

Assuming that only a single isomer population exists, the comparison of the experimental and calculated energy splittings can be used to identify a best match among different candidate structures. Experimentally, as stated above, the 2-fold split $^7F_2$ level displays a linear increase in the emission energy of the higher band component with increasing alkali metal ionic radius and a concave dependence for the low energy band component. The C_1 structure (Figure 6d) can therefore be ruled out because: (i) its high energy band component is itself significantly split for Li and Na (with the mean of this splitting decreasing with ionic radius) whereas (ii) the low energy band component monotonically increases in contrast to our observation. For the C_2 structures (Figure 6c), the higher energy band component decreases and the lower energy band component shows a convex dependence on the ionic radius unlike what is observed experimentally. Finally the high energy band component of the C_3 structures (Figure 6b) increases monotonically (almost linearly) whereas the low energy band component displays a concave dependence on the alkali metal ionic radii. Therefore, although the absolute magnitude of the splitting is currently not accurately reproduced by any of the calculations, the experimental trend from Li to Cs is best explained by a coordination shell with C_3 symmetry (Figure 6a,b). Additionally, the C_3 structures correspond to the lowest energy isomers found at the B-P/def2-TZVPP level of theory. We therefore conclude that the ions probed most likely consisted of C_3 isomers.

A luminescence sensitization pathway typical for complexes like those studied herein, would involve a ligand triplet donor state.[48] However, the experimentally determined triplet energy of the free neutral 9-hydroxyphenalen-1-one ($T_1 - S_0$ = 17 350 cm^{-1}) is almost resonant with the Eu^{3+} $^5D_0$ emission level ($^5D_0 - {}^7F_0$ = 17250 cm^{-1}). As extensively discussed for condensed-phase experiments, such a small energy difference (<2000 cm^{-1}) between the T_1 energy level of the ligand and the $^5D_0$ emitting level of the europium cation is considered unfavorable for excitation transfer due to the possibility of a back energy transfer to the triplet state.[13] This does not necessarily preclude energy transfer from a ligand based triplet state in the gas phase because at 85 K, kT is only ~59 cm^{-1} and both the coordination of the europium as well as binding of the different alkali metals by the coordinating oxygen atoms of the ligands will lead to energy level shifts relative to the free ligand. Conceivably, potential energy donating levels, e.g., the HPLN T_1 state, can be significantly upshifted by alkali metal cation complexation in gas phase, thereby affecting sensitization.[79] Another possible excitation mechanism could involve the direct excitation of the Eu^{3+} $^5D_2 \rightarrow {}^7F_0$ transition (~21 470 $cm^{-1} \cong$ 466 nm), for example, via a dynamic-coupling or ligand polarization mechanism.[80]

Finally, although the complexes with small cations, such as Li and Na, are found to be qualitatively brighter, a more quantitative comparison of their relative photoluminescence quantum yields requires optimal excitation of each complex. This and associated studies of gas-phase absorption spectra will follow in a subsequent paper.

CONCLUSION

In short, alkali metal cationization of $[Eu(PLN)_3]$ in the gas phase appears to enhance europium sensitization by the 9-hydroxy-phenal-1-one ligand with the enhancement being most effective for lithium and sodium. Corresponding measurements of the photoluminescence of mass selected $[Eu(PLN)_3M]^+$ species (M = Li, Na, K, Rb, and Cs) in the gas phase show a 2-fold split of the $^5D_0 \rightarrow {}^7F_2$ hypersensitive band. While the higher energy emission component undergoes a linear blue shift, the lower energy component undergoes an apparent quadratic shift as a function of the alkali metal ionic radius. These effects are best explained by the ligand fields of the computed C_3 symmetry structures. In combination with the experimental approach described, further refinements of the theoretical model used to calculate the energy level splittings of

dx.doi.org/10.1021/jp4086624 | J. Phys. Chem. A 2014, 118, 94−102

europium(III) ions would offer a unique tool to study the coordination shell and optical properties of a wider range of lanthanoid systems with well-defined stoichiometry. Gas-phase luminescence lifetimes will be reported in a subsequent paper. Ultimately, the aim is to gain a better insight on intramolecular energy transfers mechanisms with a special focus on the luminescence properties of hetero multinuclear lanthanoid complexes.

■ ASSOCIATED CONTENT

Supporting Information

Negative ion mode MS spectrum, ^{1}H NMR spectra, emission band energies vs the ionic radius of the alkali metal, Figure 6 with intensity scales, luminescence excitation/emission map, and coordinates of the ground state and excited states of the complexes investigated. This material is available free of charge via the Internet at http://pubs.acs.org.

■ AUTHOR INFORMATION

Corresponding Authors

*J.-F. Greisch: e-mail, jean-francois.greisch@kit.edu.
*D. Schooss: e-mail, detlef.schooss@kit.edu.

Notes

The authors declare no competing financial interest.

■ ACKNOWLEDGMENTS

We acknowledge support from the Deutsche Forschungsgemeinschaft (DFG) as administered by the transregional collaborative research center SFB/TRR 88 "3MET" (C1, C5, and C7). We are also grateful to the Bundesministerium für Bildung und Forschung (BMBF) through the Helmholtz Research Program POF "Science and Technology of Nanosystems" and to the State of Baden-Württemberg for providing the necessary infrastructure. Access to a prerelease version of McPHASE (4.9) *ic1ion* and correspondence with Dr. Manh Duc Le is acknowledged. J.F.G. acknowledges support from the Alexander von Humboldt Foundation.

■ REFERENCES

(1) Coppo, P.; Duati, M.; Kozhevnikov, V. N.; Hofstraat, J. W.; De Cola, L. White-Light Emission from an Assembly Comprising Luminescent Iridium and Europium Complexes. *Angew. Chem., Int. Ed. Engl.* **2005**, *44*, 1806−1810.
(2) Kido, J.; Okamoto, Y. Organo Lanthanide Metal Complexes for Electroluminescent Materials. *Chem. Rev. (Washington, DC, U. S.)* **2002**, *102*, 2357−2368.
(3) Wegh, R. T.; Donker, H.; Oskam, K. D.; Meijerink, A. Visible Quantum Cutting in LiGdF4:Eu3+ Through Downconversion. *Science* **1999**, *283*, 663−666.
(4) Kodama, N.; Oishi, S. Visible Quantum Cutting through Downconversion in KLiGdF5:Eu3+ Crystals. *J. Appl. Phys. (Melville, NY, U. S.)* **2005**, *98*, 103515−1−5.
(5) Moore, E. G.; Samuel, A. P. S.; Raymond, K. N. From Antenna to Assay: Lessons Learned in Lanthanide Luminescence. *Acc. Chem. Res.* **2009**, *42*, 542−552.
(6) Piguet, C.; Rivara-Minten, E.; Bernardinelli, G.; Bünzli, J. C. G.; Hopfgartner, G. Non-Covalent Lanthanide Podates with Predetermined Physicochemical Properties: Iron(II) Spin-State Equilibria in Self-Assembled Heterodinuclear d−f Supramolecular Complexes. *J. Chem. Soc., Dalton Trans.* **1997**, 421−433.
(7) Sabbatini, N.; Guardigli, M.; Lehn, J. M. Luminescent Lanthanide Complexes as Photochemical Supramolecular Devices. *Coord. Chem. Rev.* **1993**, *123*, 201−228.
(8) Choppin, G. R.; Peterman, D. R. Applications of Lanthanide Luminescence Spectroscopy to Solution Studies of Coordination Chemistry. *Coord. Chem. Rev.* **1998**, *174*, 283−299.
(9) Weissman, S. I. Intramolecular Energy Transfer The Fluorescence of Complexes of Europium. *J. Chem. Phys.* **1942**, *10*, 214−217.
(10) Dexter, D. L. A Theory of Sensitized Luminescence in Solids. *J. Chem. Phys.* **1953**, *21*, 836−850.
(11) Crosby, G. A.; Whan, R. E.; Alire, R. M. Intramolecular Energy Transfer in Rare Earth Chelates. Role of the Triplet State. *J. Chem. Phys.* **1961**, *34*, 743−748.
(12) Klink, S. I.; Grave, L.; Reinhoudt, D. N.; van Veggel, F. C. J. M.; Werts, M. H. V.; Geurts, F. A. J.; Hofstraat, J. W. A Systematic Study of the Photophysical Processes in Polydentate Triphenylene-Functionalized Eu3+, Tb3+, Nd3+, Yb3+, and Er3+ Complexes. *J. Phys. Chem. A* **2000**, *104*, 5457−5468.
(13) Beeby, A.; Faulkner, S.; Parker, D.; Williams, J. A. G. Sensitised Luminescence from Phenanthridine Appended Lanthanide Complexes: Analysis of Triplet Mediated Energy Transfer Processes in Terbium, Europium and Neodymium Complexes. *J. Chem. Soc., Perkin Trans. 2* **2001**, 1268−1273.
(14) Klink, S. I.; Hebbink, G. A.; Grave, L.; Oude Alink, P. G. B.; van Veggel, F. C. J. M.; Werts, M. H. V. Synergistic Complexation of Eu3+ by a Polydentate Ligand and a Bidentate Antenna to Obtain Ternary Complexes with High Luminescence Quantum Yields. *J. Phys. Chem. A* **2002**, *106*, 3681−3689.
(15) Gonçalves e Silva, F. R.; Malta, O. L.; Reinhard, C.; Güdel, H. U.; Piguet, C.; Moser, J. E.; Bünzli, J. C. G. Visible and Near-Infrared Luminescence of Lanthanide-Containing Dimetallic Triple-Stranded Helicates: Energy Transfer Mechanisms in the SmIII and YbIII Molecular Edifices. *J. Phys. Chem. A* **2002**, *106*, 1670−1677.
(16) Hebbink, G. A.; Grave, L.; Woldering, L. A.; Reinhoudt, D. N.; van Veggel, F. C. J. M. Unexpected Sensitization Efficiency of the Near-Infrared Nd3+, Er3+, and Yb3+ Emission by Fluorescein Compared to Eosin and Erythrosin. *J. Phys. Chem. A* **2003**, *107*, 2483−2491.
(17) El-ghayoury, A.; Harriman, A.; Ziessel, R. Intercompartmental Electron Exchange in Geometrically-Constrained Ru-Os Triads Built around Diethynylated Aryl Hydrocarbons. *J. Phys. Chem. A* **2000**, *104*, 7906−7915.
(18) Scholes, G. D. Long-Range Resonance Energy Transfer in Molecular Systems. *Annu. Rev. Phys. Chem.* **2003**, *54*, 57−87.
(19) Werts, M. H. V.; Duin, M. A.; Hofstraat, J. W.; Verhoeven, J. W. Bathochromicity of Michler's Ketone upon Coordination with Lanthanide(III) B-Diketonates Enables Efficient Sensitisation of Eu3+ for Luminescence under Visible Light Excitation. *J. Chem. Soc., Chem. Commun.* **1999**, 799−800.
(20) Kim, Y. H.; Baek, N. S.; Kim, H. K. Sensitized Emission of Luminescent Lanthanide Complexes Based on 4-Naphthalen-1-yl-Benzoic Acid Derivatives by a Charge-Transfer Process. *ChemPhysChem* **2006**, *7*, 213−221.
(21) Lazarides, T.; Alamiry, M. A. H.; Adams, H.; Pope, S. J. A.; Faulkner, S.; Weinstein, J. A.; Ward, M. D. Anthracene as a Sensitiser for Near-Infrared Luminescence in Complexes of Nd(III), Er(III) and Yb(III): an Unexpected Sensitisation Mechanism Based on Electron Transfer. *J. Chem. Soc., Dalton Trans.* **2007**, 1484−1491.
(22) Nie, D.; Chen, Z.; Bian, Z.; Zhou, J.; Liu, Z.; Chen, F. Y. Z.; Huang, C. H. Energy Transfer Pathways in the Carbazole Functionalized B-Diketonate Europium Complexes. *New J. Chem.* **2007**, *31*, 1639−1646.
(23) Kadjane, P.; Charbonnière, L.; Camerel, F.; Lainé, P. P.; Ziessel, R. Improving Visible Light Sensitization of Luminescent Europium Complexes. *J. Fluoresc.* **2008**, *18*, 119−129.
(24) D'Aléo, A.; Picot, A.; Beeby, A.; Williams, J. A. G.; Le Guennic, B.; Andraud, C.; Maury, O. Efficient Sensitization of Europium, Ytterbium, and Neodymium Functionalized Tris-Dipicolinate Lanthanide Complexes through Tunable Charge-Transfer Excited States. *Inorg. Chem.* **2008**, *47*, 10258−10268.

(25) D'Aléo, A.; Pointillart, F.; Ouahab, L.; Andraud, C.; Maury, O. Charge Transfer Excited States Sensitization of Lanthanide Emitting from the Visible to the Near-Infra-Red. *Coord. Chem. Rev.* **2012**, *256*, 1604−1620.
(26) Horrocks, W. D. W.; Bolender, J. P.; Smith, W. D.; Supkowski, R. M. Photosensitized Near Infrared Luminescence of Ytterbium(III) in Proteins and Complexes Occurs via an Internal Redox Process. *J. Am. Chem. Soc.* **1997**, *119*, 5972−5973.
(27) Beeby, A.; Faulkner, S.; Williams, J. A. G. pH Dependence of the Energy Transfer Mechanism in a Phenanthridine-Appended Ytterbium Complex. *J. Chem. Soc., Dalton Trans.* **2002**, 1918−1922.
(28) Faulkner, S.; Burton-Pye, B. P.; Khan, T.; Martin, L. R.; Wray, S. D.; Skabara, P. J. Interaction between Tetrathiafulvalene Carboxylic Acid and Ytterbium DO3A: Solution State Self-Assembly of a Ternary Complex which is Luminescent in the near IR. *J. Chem. Soc., Chem. Commun.* **2002**, 1668−1669.
(29) Klink, S. I.; Keizer, H.; van Veggel, F. C. J. M. Transition Metal Complexes as Photosensitizers for Near-Infrared Lanthanide Luminescence. *Angew. Chem., Int. Ed.* **2000**, *39*, 4319−4321.
(30) Klink, S. I.; Keizer, H.; Hofstraat, H. W.; van Veggel, F. C. J. M. Transition Metal Complexes as a New Class of Photosensitizers for Near-Infrared Lanthanide Luminescence. *Synth. Met.* **2002**, *127*, 213−216.
(31) Miller, T. A.; Jeffery, J. C.; Ward, M. D.; Adams, H.; Pope, S. J. A.; Faulkner, S. Photoinduced Ru−Yb Energy Transfer and Sensitised near-IR Luminescence in a Coordination Polymer Containing Co-Crystallised [Ru(bipy)(CN)4]2 and Yb(III) Units. *J. Chem. Soc., Dalton Trans.* **2004**, 1524−1526.
(32) Sénéchal-David, K.; Pope, S. J. A.; Quinn, S.; Faulkner, S.; Gunnlaugsson, T. Sensitized Near-Infrared Lanthanide Luminescence from Nd(III)- and Yb(III)-Based Cyclen-Ruthenium Coordination Conjugates. *Inorg. Chem.* **2006**, *45*, 10040−10042.
(33) Ziessel, R.; Diring, S.; Kadjane, P.; Charbonnière, L.; Retailleau, P.; Philouze, C. Highly Efficient Blue Photoexcitation of Europium in a Bimetallic Pt−Eu Complex. *Chem. - Asian J.* **2007**, *2*, 975−982.
(34) Chen, F. F.; Bian, Z. Q.; Liu, Z. W.; Nie, D. B.; Chen, Z. Q.; Huang, C. H. Highly Efficient Sensitized Red Emission from Europium (III) in Ir-Eu Bimetallic Complexes by 3MLCT Energy Transfer. *Inorg. Chem.* **2008**, *47*, 2507−2513.
(35) Förster, T. Zwischenmolekulare Energiewanderung und Fluoreszenz. *Ann. Phys. (Berlin, Ger.)* **1948**, *437*, 55−75.
(36) Imbert, D.; Cantuel, M.; Bunzli, J. C. G.; Bernardinelli, G.; Piguet, C. Extending Lifetimes of Lanthanide-Based Near-Infrared Emitters (Nd, Yb) in the Millisecond Range through Cr(III) Sensitization in Discrete Bimetallic Edifices. *J. Am. Chem. Soc.* **2003**, *125*, 15698−15699.
(37) Torelli, S.; Imbert, D.; Cantuel, M.; Bernardinelli, G.; Delahaye, S.; Hauser, A.; Bunzli, J. C. G.; Piguet, C. Tuning the Decay Time of Lanthanide-Based Near Infrared Luminescence from Micro- to Milliseconds through d->f Energy Transfer in Discrete Heterobimetallic Complexes. *Chem. - Eur. J.* **2005**, *11*, 3228−3242.
(38) Sayre, E. V.; Freed, S. Spectra and Quantum States of the Europic Ion in Crystals. II. Fluorescence and Absorption Spectra of Single Crystals of Europic Ethylsulfate Nonahydrate. *J. Chem. Phys.* **1956**, *24*, 1213−1219.
(39) van Vleck, J. H. The Puzzle of Rare-Earth Spectra in Solids. *J. Phys. Chem.* **1937**, *41*, 67−80.
(40) Broer, L. J. F.; Gorter, C. J.; Hoogschagen, J. On the Intensities and the Multipole Character in the Spectra of the Rare Earth Ions. *Physica XI* **1945**, *11*, 231−250.
(41) Walsh, B. M., *Advances in Spectroscopy for Lasers and Sensing*; Di Bartolo, B., Forte, O., Eds.; Springer: The Netherlands, 2006; pp 403−433.
(42) Judd, B. R. Optical Absorption Intensities of Rare-Earth Ions. *Phys. Rev.* **1962**, *127*, 750−761.
(43) Ofelt, G. S. Intensities of Crystal Spectra of RareEarth Ions. *J. Chem. Phys.* **1962**, *37*, 511−520.
(44) Wybourne, B. G. Effective Operators and Spectroscopic Properties. *J. Chem. Phys.* **1968**, *48*, 2596−2611.
(45) Lowther, J. E. Spectroscopic Transition Probabilities of Rare Earth Ions. *J. Phys. C: Solid State Phys.* **1974**, *7*, 4393−4402.
(46) Jankowski, K.; Sokolowski, A. Ab Initio Studies of Electron Correlation in Rare-Earth Ions. I. Intrashell Correlation for 4f2 in Pr3+. *J. Phys. B: At. Mol. Phys.* **1981**, *14*, 3345−3353.
(47) Downer, M. C.; Burdick, G. W.; Sardar, D. K. A New Contribution to Spinforbidden Rare Earth Optical Transition Intensities: Gd3+ and Eu3+. *J. Chem. Phys.* **1988**, *89*, 1787−1797.
(48) Bünzli, J. C. G.; Piguet, C. Taking Advantage of Luminescent Lanthanide Ions. *Chem. Soc. Rev.* **2005**, *34*, 1048−1077.
(49) Eliseeva, S. V.; Bünzli, J. C. G. Lanthanide Luminescence for Functional Materials and Bio-Sciences. *Chem. Soc. Rev.* **2010**, *39*, 189−227.
(50) Haddon, R. C.; Rayford, R.; Hirani, A. M. 2-Methyl- and 5-Methyl-9-Hydroxyphenalenone. *J. Org. Chem.* **1981**, *46*, 4587−4588.
(51) Bondybey, V. E.; Haddon, R. C.; English, J. H. Fluorescence and Phosphorescence of 9-Hydroxyphenalenone in Solid Neon and its Hydrogen Tunneling Potential Function. *J. Chem. Phys.* **1984**, *80*, 5432−5437.
(52) Van Deun, R.; Nockemann, P.; Fias, P.; Van Hecke, K.; Van Meervelt, L.; Binnemans, K. Visible Light Sensitisation of Europium(III) Luminescence in a 9-Hydroxyphenal-1-one Complex. *J. Chem. Soc., Chem. Commun.* **2005**, 590−592.
(53) Greisch, J. F.; Harding, M. E.; Kordel, M.; Klopper, W.; Kappes, M. M.; Schooss, D. Intrinsic Fluorescence Properties of Rhodamine Cations in Gas-Phase: Triplet Lifetimes and Dispersed Fluorescence Spectra. *Phys. Chem. Chem. Phys.* **2013**, *15*, 8162−8170.
(54) Wang, Y.; Hendrickson, C. L.; Marshall, A. G. Direct Optical Spectroscopy of Gas-Phase Molecular Ions Trapped and Mass-Selected by Ion Cyclotron Resonance: Laser-Induced Fluorescence Excitation Spectrum of Hexafluorobenzene (C6F6+). *Chem. Phys. Lett.* **2001**, *334*, 69−75.
(55) Frankevich, V.; Guan, X.; Dashtiev, M.; Zenobi, R. Laser-Induced Fluoresence of Trapped Gas-Phase Molecular Ions Generated by Internal-Source Matrix-Assisted Laser Desorption/Ionization in a Fourier Transform Ion Cyclotron Resonance Mass Spectrometer. *Eur. J. Mass Spectrom.* **2005**, *11*, 475−482.
(56) Friedrich, J.; Fu, J.; Hendrickson, C. L.; Marshall, A. G.; Wang, Y. S. Time Resolved Laser-Induced Fluorescence of Electrosprayed Ions Confined in a Linear Quadrupole Trap. *Rev. Sci. Instrum.* **2004**, *75*, 4511−4515.
(57) Khoury, J. T.; Rodriguez-Cruz, S. E.; Parks, J. H. Pulsed Fluorescence Measurements of Trapped Molecular Ions with Zero Background Detection. *J. Am. Soc. Mass Spectrom.* **2002**, *13*, 696−708.
(58) Sassin, N.; Everhart, S.; Dangi, B.; Ervin, K.; Cline, J. Fluorescence and Photodissociation of Rhodamine 575 Cations in a Quadrupole Ion Trap. *J. Am. Soc. Mass Spectrom.* **2009**, *20*, 96−104.
(59) McQueen, P. D.; Sagoo, S.; Yao, H.; Jockusch, R. A. On the Intrinsic Photophysics of Fluorescein. *Angew. Chem., Int. Ed.* **2010**, *49*, 9193−9196.
(60) Kordel, M.; Schooss, D.; Neiss, C.; Walter, L.; Kappes, M. M. Laser-Induced Fluorescence of Rhodamine 6G Cations in the Gas Phase: A Lower Bound to the Lifetime of the First Triplet State. *J. Phys. Chem. A* **2010**, *114*, 5509−5514.
(61) Van Deun, R.; Fias, P.; Nockemann, P.; Van Hecke, K.; Van Meervelt, L.; Binnemans, K. Visible-Light-Sensitized Near-Infrared Luminescence from Rare-Earth Complexes of the 9-Hydroxyphenalen-1-one Ligand. *Inorg. Chem.* **2006**, *45*, 10416−10418.
(62) Freire, R. O.; Simas, A. M. Sparkle/PM6 Parameters for all Lanthanide Trications from La(III) to Lu(III). *J. Chem. Theory Comput.* **2010**, *6*, 2019−2023.
(63) Becke, A. D. Density-Functional Exchange-Energy Approximation with Correct Asymptotic Behavior. *Phys. Rev. A: At., Mol., Opt. Phys.* **1988**, *38*, 3098−3100.
(64) Gulde, R.; Pollak, P.; Weigend, F. Error-Balanced Segmented Contracted Basis Sets of Double-ζ to Quadruple-ζ Valence Quality for the Lanthanides. *J. Chem. Theory Comput.* **2012**, *8*, 4062−4068.
(65) Weigend, F.; Ahlrichs, R. Balanced Basis Sets of Split Valence, Triple Zeta Valence and Quadruple Zeta Valence Quality for H to Rn:

Design and Assessment of Accuracy. *Phys. Chem. Chem. Phys.* **2005**, *7*, 3297−3305.
(66) Weigend, F.; Häser, M.; Patzelt, H.; Ahlrichs, R. RI-MP2: Optimized Auxiliary Basis Sets and Demonstration of Efficiency. *Chem. Phys. Lett.* **1998**, *294*, 143−152.
(67) *TURBOMOLE V6.4 2012, a development of University of Karlsruhe and Forschungszentrum Karlsruhe GmbH, 1989−2007, TURBOMOLE GmbH, since 2007*; available from http://www.turbomole.com.
(68) Weigend, F. Accurate Coulomb-Fitting Basis Sets for H to Rn. *Phys. Chem. Chem. Phys.* **2006**, *8*, 1057−1065.
(69) Walsh, B. M., Judd-Ofelt Theory: Principles and Practices. In *Advances in Spectroscopy for Lasers and Sensing*; Di Bartolo, B., Forte, O., Eds.; Springer: Netherlands, 2006; pp 403−433.
(70) Bünzli, J. C. G.; Eliseeva, S. V. Basics of Lanthanide Photophysics. In *Lanthanide Luminescence: Photophysical, Analytical and Biological Aspects*; Hänninen, P., Härmä, H., Eds.; Springer-Verlag: Berlin, Heidelberg, 2010.
(71) Rotter, M.; Duc Le, M.; Boothroyd, A. T.; Blanco, J. A. Dynamical Matrix Diagonalization for the Calculation of Dispersive Excitations. *J. Phys.: Condens. Matter* **2012**, *24*, 213201−1−23.
(72) Reed, A. E.; Weinstock, R. B.; Weinhold, F. Natural Population Analysis. *J. Chem. Phys.* **1985**, *83*, 735−746.
(73) Oliferenko, A. A.; Palyulin, V. A.; Pisarev, S. A.; Neiman, A. V.; Zefirov, N. S. Novel Point Charge Models: Reliable Instruments for Molecular Electrostatic. *J. Phys. Org. Chem.* **2001**, *14*, 355−369.
(74) Guan, S. H.; Marshall, A. G. Stored Wave-Form Inverse Fourier-Transform Axial Excitation/Ejection for Quadrupole Ion-Trap Mass-Spectrometry. *Anal. Chem.* **1993**, *65*, 1288−1294.
(75) Foster, D. R.; Richardson, F. S. Magnetic Circularly Polarized Luminescence Spectra of 9-Coordinate Europium(III) Complexes in Aqueous Solution. *Inorg. Chem.* **1983**, *22*, 3996−4002.
(76) Walton, J. W.; Carr, R.; Evans, N. H.; Funk, A. M.; Kenwright, A. M.; Parker, D.; Yufit, D. S.; Botta, M.; De Pinto, S.; Wong, K. L. Isostructural Series of Nine-Coordinate Chiral Lanthanide Complexes Based on Triazacyclononane. *Inorg. Chem.* **2012**, *51*, 8042−8056.
(77) Conway, B. E.; Ayranci, E. Effective Ionic Radii and Hydration Volumes for Evaluation of Solution Properties and Ionic Adsorption. *J. Solution Chem.* **1999**, *28*, 163−192.
(78) Rotter, M. Using McPhase to Calculate Magnetic Phase Diagrams of Rare Earth Compounds. *J. Magn. Magn. Mater.* **2004**, *272−276*, E481−E482.
(79) Zhuravlev, K.; Tsaryuk, V.; Kudryashova, V.; Zolin, V.; Yakolev, Y.; Legendziewicz, J. Optical Spectroscopy of Europium 3,5-Dinitrosalicylates-Intense Red Luminophores. *Spectrochim. Acta, Part A* **2009**, *72*, 1020−1025.
(80) Hatanaka, M.; Yabushita, S. Theoretical Study on the f-f Transition Intensities of Lanthanide Trihalide Systems. *J. Phys. Chem. A* **2009**, *113*, 12615−12625.